Humanoid HRP2-DHRC for Autonomous and Interactive Behavior

S. Kagami[1,2], K. Nishiwaki[1,2], J. Kuffner[3,1], S. Thompson[1], J. Chestnutt[3], M. Stilman[3], P. Michel[3]

[1] Digital Human Research Center, AIST. `s.kagami@aist.go.jp`
[2] CREST Program, JST.
[3] Robotics Institute, Carnegie-Mellon University.

1 Introduction

Recently, research on humanoid-type robots has become increasingly active, and a broad array of fundamental issues are under investigation. However, in order to achieve a humanoid robot which can operate in human environments, not only the fundamental components themselves, but also the successful integration of these components will be required. At present, almost all humanoid robots that have been developed have been designed for bipedal locomotion experiments. In order to satisfy the functional demands of locomotion as well as high-level behaviors, humanoid robots require good mechanical design, hardware, and software which can support the integration of tactile sensing, visual perception, and motor control. Autonomous behaviors are currently still very primitive for humanoid-type robots. It is difficult to conduct research on high-level autonomy and intelligence in humanoids due to the development and maintenance costs of the hardware. We believe low-level autonomous functions will be required in order to conduct research on higher-level autonomous behaviors for humanoids.

This paper describes our research efforts aimed at developing low-level autonomous capabilities required for moving & manipulation tasks involving humanoid-type robots. In that purpose, Humanoid HRP2-DHRC(Fig.1) is designed by improved from original HRP2[1] to have extra joints and sensors, and it is manufactured by Kawada Industries Inc. On this platform, sense-plan-act loop is implemented for autonomous moving & manipulation. Augmented reality based humanoid robot experiment system is also developed to help developing each functions.
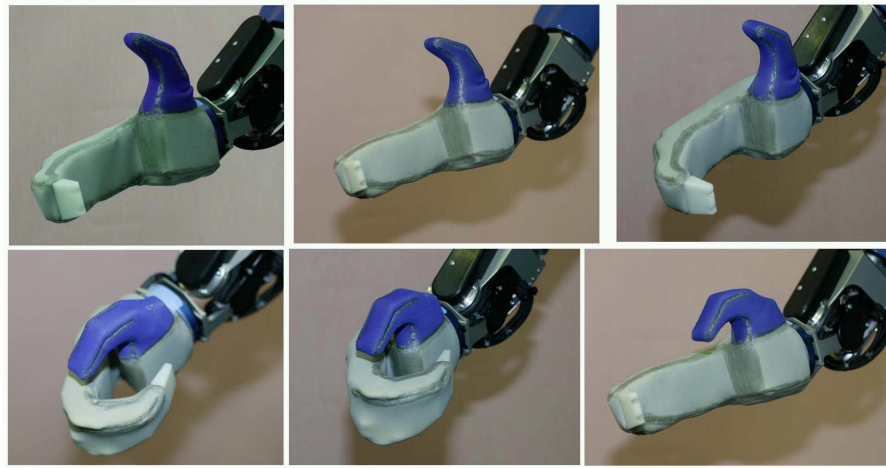
Fig. 1. Humanoid HRP2-DHRC

Fig. 2. Hand postures of HRP2-DHRC

2 Humanoid HRP2-DHRC Hardware Improvements

2.1 Additional Joints

Original HRP2 has 30 DOF in total (6 DOF for arm & leg, 2 DOF for neck & waist, 1 DOF for gripper). There are three part that joints added for HRP2-
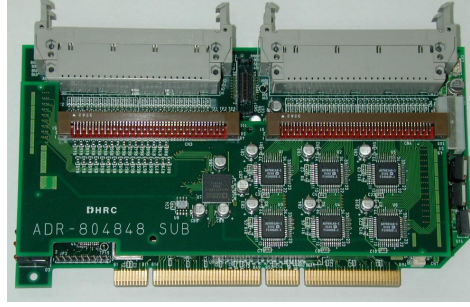
Fig. 3. DHRC-ADR804848: PCI half size IO board

DHRC: 1) wrist, 2) hand and 3) toe. HRP2-DHRC has 38 DOF in total and it is 158cm in height & 58kg in weight(Fig.1).

As for 1) arm, in order to increase high manipulability region, 1 DOF is added at wrist joint. As for 2) hand, 3 DOF hand that can grasp objects in several different ways is designed by Prof. Inoue and attached to Humanoid JSK-H7[2]. We adopted the same mechanisms to HRP2-DHRC(Fig.2). As for 3) foot, 1 DOF is added at toe in order to improve walking motion as like H7.

2.2 Control Board

An PCI I/O board is newly developed to achieve current sensor based torque control(Fig.3). The board has 80ch AD(14bit), 48ch DA(12bit) & encoder counter, 32ch DIO. It can achieve up to 10khz sampling for all input/output usage situation (up to 48 joints) by using DMA data transmission through 32bit/64bit PCI bus. Current sensor signal of motor driver is connected to AD input, so that torque control is possible. Board has almost 1 slot PCI half size.

2.3 Head Sensor

Original HRP2 has three synchronized mono cameras at head. Firewire (IEEE1394) stereo camera Videre design STH-DCGS is adopted together with time of flight type laser range sensor Hokuyo URG-04LX at head. Videre design STH-DCGS has global shuttered VGA stereo camera and has about 90 degrees view angle in horizontal.

URG-04LX is a small (160g) range sensor that measures up to 4m and covers 270 degrees in 0.36 degrees resolution.

2.4 Experimental Sensor

Foot force distribution sensor and HD resolution stereo camera are under developing functions for humanoid robots.
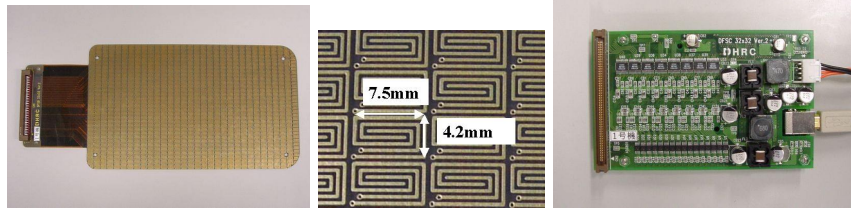
Fig. 4. Electrode part of the sensor, its sensing area close up and IO board

Foot Force Distribution Sensor

Scanning Circuit

A 32×32 matrix scan type high-speed pressure sensor for the feet of humanoid robots that has 1[kHz] sampling rate is developed(Fig.4). This sensor has matrix scan circuit. The matrix scan method has a problem of interference by bypass current. In order to resolve this problem, a novel method is proposed.

We adopted very thin(0.6[mm]) force sensing conductive rubber sheet for high speed sensing. Each sensing area is 4.2×7.0[mm] and can measure vertical force of approximately 0.25–20[N]. Walking cycle of humanoid robot as well as human being is about 0.4–0.8[s] and dual leg phase is about 0.1–0.15[s]. The target of the sensor is biped walk stabilization so that high-speed input is important. Matrix scan type circuit is connected to sensor, and the system runs 1[kHz] with 14[bit] resolution at 4.2×7.0[mm] grid for 32×32 points, and the sensor size is the same as humanoid robot foot 135×228[mm]. The system is running high-speed because of very thin conductive rubber and simultaneous measurement.

Electrodes which are shown in Fig.4 are arranged in the shape of a grid. There is a flexible cable part which has connector at the left side of electrode part to avoid collision to the ground and robot itself is important. The control circuit board is attached to the shank link of our humanoid robot H7, and only USB2 cable goes through the joints to the controlling PC mounted on the torso.

Thin force sensing rubber

Thickness of developed force sensing rubber is 0.6[mm] (Inaba Instries Inc.). Conductive carbon composite grain are mixed in the rubber. Thinness is better to achieve small time constant and sensitivity, so that system can realize higher scan rate. Table.1 shows a specification of our rubber sheet.

With no load, resistance on a surface and on a volume are both about $10^7[\Omega]$. As the pressure is exerted, rubber deforms and conductive path augments, so that relationship in between pressure and registance changes monotonic and smooth.
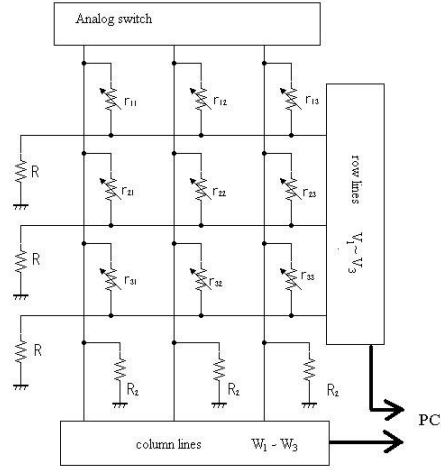
Fig. 5. Pressure sensor circuit diagram. (Example 3x3 matrix)

Fig. 6. Humanoid robot foot with pressure sensor grid and human foot pressure result

The usual matrix scan method is equipped with AD converters on the column lines. The system in this paper is equipped AD converters both on the column lines and row lines of the sensor matrix(Fig.5). When the column line 1 is applied the voltage, the following formula is led from Kirchhoff's current rule at the top row:

$$\frac{{}^1V_1}{R} = \sum_j \frac{{}^1W_j - {}^1V_1}{r_{1j}}.$$

Similarly, the following formula is led also about the i-th row and k-th column line:

Table 1. Force Sensing Rubber Resister

Max. Voltage	30V
Recomm. Voltage	6V
Max. Current	20mA
Recomm. Current	5mA
No-load Resistance	20MΩ
Maximum Load	100N
Recomm. Load	40N

$$\frac{^kV_i}{R} = \sum_j \frac{^kW_j - {}^kV_i}{r_{ij}}.$$

Let x_{ij} be $\frac{1}{r_{ij}}$:

$$\frac{^kV_i}{R} = \sum_j \left({}^kW_j - {}^kV_i \right) \cdot x_{ij}.$$

This formula means simultaneous equation. When $i = 1$, the formula is expressed with the following matrix:

$$\mathbf{V}_1 = M_1 \mathbf{X}_1.$$

Here, $\mathbf{V}_1, M_1, \mathbf{X}_1$ are as follows:

$$\mathbf{V}_1 = \begin{pmatrix} {}^1V_1/R \\ \vdots \\ {}^nV_1/R \end{pmatrix},$$

$$M_1 = \begin{pmatrix} {}^1W_1 - {}^1V_1 & \cdots & {}^1W_n - {}^1V_1 \\ \vdots & \ddots & \vdots \\ {}^nW_1 - {}^nV_1 & \cdots & {}^nW_n - {}^nV_1 \end{pmatrix},$$

$$\mathbf{X}_1 = \begin{pmatrix} x_{11} \\ \vdots \\ x_{1n} \end{pmatrix}.$$

Therefore $\mathbf{X}_1$ is led by using inverse matrix of M:

$$\mathbf{X}_1 = M_1^{-1} \mathbf{V}_1.$$

$$\mathbf{X}_1 = \begin{pmatrix} x_{11} \\ \vdots \\ x_{1n} \end{pmatrix} = \begin{pmatrix} 1/r_{11} \\ \vdots \\ 1/r_{1n} \end{pmatrix}$$

Similarly, i-th $\mathbf{X}_i$ is calculated.

$$\mathbf{X}_i = M_i^{-1}\mathbf{V}_i = \begin{pmatrix} 1/r_{i1} \\ \vdots \\ 1/r_{in} \end{pmatrix}$$

Value of resistance r_{ij} is found by taking the reciprocal of each element of vector $\mathbf{X}_i$.

Experimental results

Dynamic pressure was applied to the sensor(Fig.6(right)). As the dynamic pressure, the subject(male, weight:65kg, foot size:27cm) run on the sensor. Scanning rate was 300[Hz].

The pressure sensor is attached to our humanoid robot H7 foot(Fig.6. Distributed pressure is measured and COP trajectory is calculated.

Developed thin force sensing conductive resistance rubber has about 1500-1[Ω] at 0.25-20[N]. Matrix scan is achieved with a novel method. Resistance at each sensing point is calculated by solving the simultaneous equations from column and row lines voltage. Interference by bypass current is suppressed by this method. The result of load and output voltage is monotonic, and doesn't have large hysteresis. The high-speed(1[kHz]) sensor was realized by measuring voltage simultaneously and thin(0.6[mm]) force sensing conductive rubber.

HD Stereo Camera

Humanoid vision sometimes requires to have multi-resolution or zooming function. For example, avoiding obstacles, looking for a path to given goal, detecting human posture, such tasks requires to have wide view angle. However, finding face, detecting grasping position of target object, measuring distance to next step, such tasks requires to have narrow view angle to measure precise accuracy.

There exists several humanoid systems that have two (or more) stereo camera sets which has different lenses. However, alignment of those multiple stereo camera causes difficult problem. Also data bus speed is another limitation.

In order to overcome these problem, we developed stereo camera that has HD resolution CMOS, and simultaneously captures use whole image (but subsampled) and dense image at desired position (such as center) (Fig.7).

Imager is Altasens ProCamHD3560 (2/3" CMOS) that has 1920×1080 in 60P global shutter. We also developed C-mount HD resolution lens of f=4.8mm (about 90deg). This lens has HD resolution at fringe. This camera is connected to PC by using USB2 bus. Bandwidth of USB2 bus is not sufficient to handle HD 60P raw color image. Therefore, we prepare dual CIF/VGA

Fig. 7. HD stereo camera, whole image, and 320x240 left upper corner image

resolution stereo mode that captures two stereo pair of 1) full screen (sub-sampled) and 2) dense partial image (about 15 degrees). In CIF mode, the camera achieves 60Hz capturing. The camera size is 195x85x65[mm], weight is 225[g] and consumes about 10[W].

3 Augmented Reality based Development System

In order to develop more sophisticated autonomous humanoid behaviors, thorough testing of various interconnected hardware and software components for sense, plan and control becomes increasingly difficult. Many software tools are available for dynamic simulation and visualization in simulation stage. However, when robots are put to the test in real environments these tools are only used offline for processing the data of an experiment. We encountered difficulty to achieve real-world autonomy even after developing each sense-plan-act functions. There are problems such as follows: a) perception error (accuracy, repeatability) is hard to examine because of the lack of global information such as relationship between robot and environment, b) planning and control software error caused by particular perception are hard to found because of lack of repeatability, c) planning and control software tuning are also difficult.

We propose an alternate paradigm for real-world experimentation that utilizes a real-time optical tracking system to form a complete hybrid real/virtual testing environment.

Our proposed system has two objectives: to present the researcher with a ground truth model of the world and to introduce virtual objects into actual real world experiments. Conceptually it is real bi-directional augmented reality.

To see the relevance of these tools, consider an example of how the proposed system is used in our laboratory. A humanoid robot with algorithms for vision, path planning and ZMP stabilization is given the task of navigation in a field of obstacles. During an online experiment, the robot unexpectedly contacts one of the obstacles. Did our vision system properly construct a model of the environment? Did the navigation planner find an erroneous path? Was our controller properly following the desired trajectory? A ground truth

model helps resolve ambiguities regarding the source of experimental failures by precisely identifying the locations of the obstacles and the robot. Just as in simulation, we can immediately determine whether the vision algorithm identified the model, or whether the controller followed the trajectory designed by the planner. In some cases, we can avoid the undesired interaction entirely. Having established a correspondence between virtual components such as environment models, plans, intended robot actions and the real world, we can then visualize and identify system errors prior to their occurrence.

In this section, we describe the implementation of the hybrid experimental environment. We develop tools for constructing a correspondence between real and virtual worlds. Using these tools we find substantial opportunities for experimentation by introducing virtual obstacles, virtual sensors and virtual robots into a real world environment. We describe how adding such objects to an experimental setting aids in the development and thorough testing of vision, planning and control[3].

3.1 System Configuration

To construct a hybrid real/virtual environment, we instrumented our lab space with the Eagle-4 Motion Analysis motion capture system. The environment also contains cameras and furniture objects. Our experiments focused on high level autonomous tasks for the humanoid robot HRP-2. For instance, the robot navigated the environment while choosing foot locations to avoid obstacles and manipulated obstacles to free its path. We partitioned these experiments according to the subsystems of vision, planning and control to provide a general groundwork for how a hybrid real/virtual testing environment can be used in a larger context of research objectives.

The Eagle-4 system consists of 12 cameras, covering a space of $5 \times 5 \times 1.8$ meters. Distances between markers that appear in this space can be calculated to 0.3% accuracy. In our experiments, the motion capture estimate of the distance between two markers at an actual distance of 300mm has less than 1mm error.

In terms of processing speed, we employ a dual Xeon 3.6GHz processor computer to collect the motion capture information. The EVa Real-Time Software (EVaRT) registers and locates 3D markers at maximum rate of 480Hz with an image resolution of 1280×1024. When larger numbers of markers are present, the maximum update speed decreases. Still, when tracking approximately 60 markers the lowest acquisition rate we used was 60Hz. Marker localization was always performed in real-time.

EVaRT groups the markers attached to an object. We refer to this set of points as the object template. Under the assumption that a group of markers is attached to a rigid object, any displacement of the object corresponds to a rigid transformation T of the markers.

During online execution, EVaRT uses distance comparisons to identify groupings of markers, as well as the identities of markers in these groupings.

Fig. 8. (a) Real chair with retroreflective markers illuminated. (b) 3D model of chair as recoverd by a laser scanner. (c) Virtual chair is overlayed in real-time. Both the chair and the camera are in motion.

We are then interested in the inverse problem of finding a transform T that aligns the template marker locations with those found in the scene by motion capture.

3.2 Geometry Reconstruction

The transformation of a rigid body's coordinate frame tells us the displacement of all points associated with the body. To reconstruct the geometry of a scene, we need to establish the geometry of each object in its local reference frame.

In our work, we have chosen to use 3D triangular surface meshes to represent environment objects. We constructed preliminary meshes using a Minolta VIVID 910 non-contact 3D laser digitizer. The meshes were manually edited for holes and automatically simplified to reduce the number of vertices.

Fig.8 demonstrates the correspondence between a chair in the lab environment and its 3D mesh in our visualization. We are able to continuously re-compute the transformation of a lab object at a rate of 30Hz. The virtual environment can then be updated in real-time to provide a visualization of the actual object's motion in the lab.

3.3 Real and Virtual Cameras

In this section we consider the latter case of placing a camera in the viewable range of motion capture. We show that tracking a camera lets us to establish a correspondence between objects in the ground truth model and objects in the camera frustum.

As with other rigid bodies, the camera is outfitted with retro-reflective markers that are grouped in EVaRT and then tracked using our algorithm. The position and orientation of the camera computed from motion capture form the extrinsic camera parameters. The translation vector t corresponds
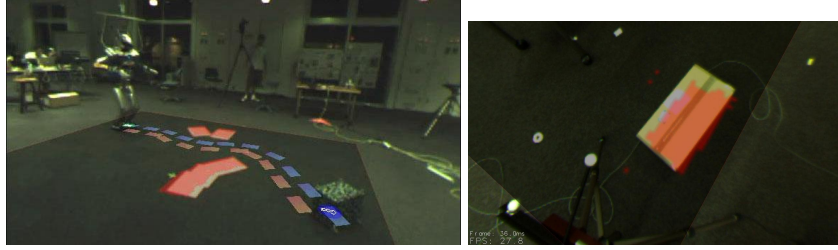
Fig. 9. Environment reconstructions overlaid onto the world. (a) Occupancy grid generated from image-based reconstruction using the robot's camera. (b) planar projection of an obstacle recovered from range data.

to the world coordinates of the camera's optical center and the 3×3 rotation matrix R represents the direction of the optical axis. Offline camera calibration using Tsai's camera model is performed once to recover the the 3×3 upper triangular intrinsic parameter matrix K. Incoming camera images can then be rectified on the fly. The extrinsic and intrinsic parameters allow us to recover the full camera projection matrix M. M uniquely maps a scene point $P = (x, y, z, 1)^T$ to a point on the image plane $p = (u, v, 1)$ T via the standard homogeneous projection equation.

Therefore, we can recover not only the locations of motion capture markers but also any points that compose the surface mesh of a tracked object.

We can use existing 3D display technology such as OpenGL to efficiently compute surface models as they would appear in the camera projection. Overlaying the virtual display on the camera display creates the a correspondence between the camera view and the ground-truth motion capture view.

3.4 Examination of Humanoid Sensing

Given a representation of the robot environment reconstructed by image warping or from range data, we can visually evaluate the accuracy of our perception algorithms and make parameter adjustments on the fly by overlaying the environment maps generated back onto a camera view of the scene. This enables us to verify that obstacles and free space in our environment reconstructions line up with their real-world counterparts, as illustrated in Fig.9.

3.5 Examination of Humanoid Planning

Fig.9(left) and Fig.10 (left) show examples of control system visualization during online robot experiments. The system has planned out the sequence of footsteps it wishes to take to reach some goal configuration. For each step, it has computed the 3D position and orientation of the foot. Through the use of augmented reality, the planned footsteps can be overlaid in real-time onto the environment.
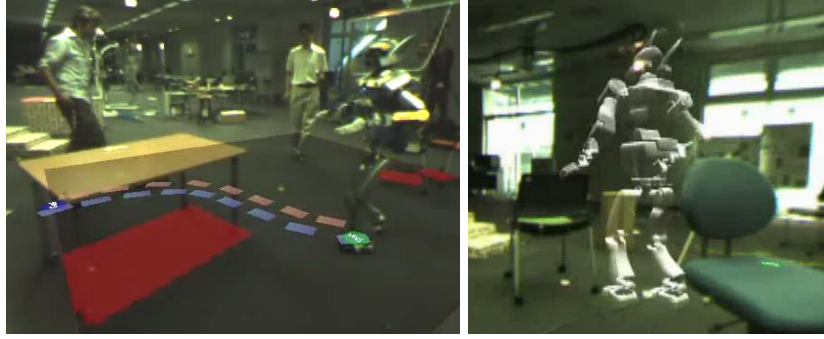
Fig. 10. Augmenting reality for visualization of planning and execution. (a) Footstep plan displayed onto the world. (b) Augmented reality with a simulated robot amongst real obstacles.

The red and blue rectangles represent the steps for the right and left feet that the robot intends to take. This path is constantly updated as the robot replans while walking. This display helps expose the planning process to identify errors and gain insight into the performance of the algorithm.

Temporal Projection: Virtual Robot

One of the components of our overall system that we would like to replace for testing purposes is the robot itself. One solution to is to build a simulated environment for experimentation. However, we would like to continue to use the real world as much as possible, rather than using a completely fabricated environment. Within our framework, we can continue to use real-world obstacles and sensors, and merely replace the robot with a simulated avatar. Fig.10 (right) shows the augmented reality of our simulated robot traversing a real environment. Note that for this navigation task, the robot is not manipulating the environment. The obstacles themselves can be moved during the experiments, but we do not need to close the loop on robotic manipulation.

Objects and the Robot's Perception

In addition to complete replacement of all sensing with perfect ground truth data, we can simulate varying degrees of realistic sensors. We can slowly increase the realism of the data which the system must handle. This approach can isolate specific sources of error, and determine to which the control system is most sensitive. For example, by knowing the locations and positions of all objects as well as the robot's sensors, we can determine which objects are detectable by the robot at any given point in time. Hence, simulated sensors can be implemented with realistic limits and coverage.
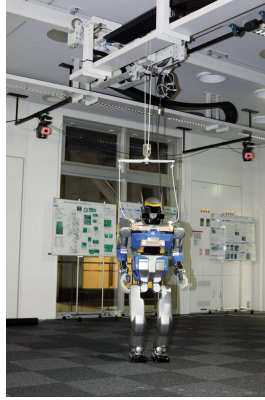
Fig. 11. Automatic following gantry & HRP2-DHRC with markers

3.6 gantry

During any task of locomotion or manipulation, a humanoid robot is at risk of falling. Typically, a small gantry is used to closely follow and secure the robot. However, the physical presence of the gantry and its operator prevent us from testing fine manipulation or navigation that requires the close proximity of objects.

To overcome this problem, our laboratory implements a ceiling suspended gantry (10×7.5[m]) that can follow the robot throughout the experimental space. It is controlled by standard PC with Timesys Linux realtime operating system (as like HRP2-DHRC). Having acquired the absolute positioning of the robot from motion capture, this gantry is PD controlled to follow the robot as it autonomously explores the space. This final component not only lets us to test the robot in arbitrary cluttered environments, but also enables experiments that typically require four or five operators to be safely performed by a single researcher.

4 Concluding Remarks

HRP2-DHRC humanoid robot is developed as a research platform for humanoid autonomy research (as like previous our H7 humanoid robot). Using HRP2-DHRC, we conducted research on sense-plan-act based humanoid autonomy as shown in Fig.12. As for "Sense" part, plane segmentation & 3D labeling[4], 6D visual odometory & world reconstruction[5], particle filter based localization[6], foot distributed force sensor[7] are studied. As for "Plan" part, footstep planning[8], arm motion planning by RRT[9], NAMO[10], manipulatibily maximization arm trajectory planning[11] are studied. As for
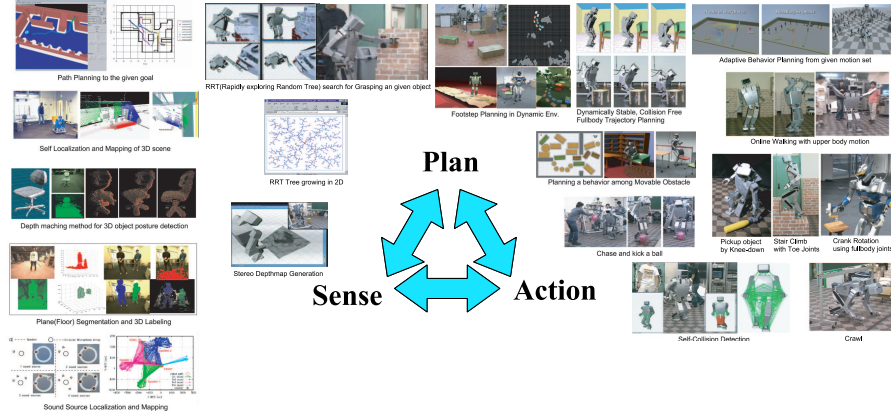
Fig. 12. Sense-Plan-Act Functions for HRP2-DHRC Low-level Autonomy

"Act" part, whole body cooperated reaching motion generation[12], whole body coordinated hand manipulation[13] are studied.

One fundamental achievement in this paper is augmented reality based development system. It is a novel experimental paradigm that leverages the recent advances in optical motion capture speed and accuracy to enable simultaneous online testing of complex robotic system components in a hybrid real-virtual world. We believe that this new approach enabled us to achieve rapid development and validation testing on each of the perception, planning, and control subsystems of our autonomous humanoid robot platform. We hope that this powerful combination of vision technology and robotics development will lead to faster realization of complex autonomous systems with a high degree of reliability.

References

1. H.Hirukawa, F.Kanehiro, K.Kaneko, S.Kajita, K.Fujiwara, Y.Kawai, F.Tomita, S.Hirai, K.Tanie, T.Isozumi, K.Akachi, T.Kawasaki, S.Ota, K.Yokoyama, H.Handa, Y.Fukase, J.Maeda, Y.Nakamura, and H.Inoue, "Humanoid Robotics Platforms Developed in HRP," *Robotics and Autonomous Systems*, vol. 48, no. 4, pp. 165–175, October 2004.
2. S. Kagami, K. Nishiwaki, J. Kuffner, K. Okada, Y. Kuniyoshi, M. Inaba, and H. Inoue, "Low-level Autonomy of Remote Operated Humanoid Robot H6 & H7," *Robotics Research*, 2003.
3. M. Stilman, P. Michel, J. Chestnutt, K. Nishiwaki, S. Kagami, and J. Kuffner, "Augmented reality for robot development and experimentation," Robotics Institute, Carnegie Mellon University, Pittsburgh, PA, Tech. Rep. CMU-RI-TR-05-55, November 2005.
4. Y. KIDA, S. KAGAMI, T. NAKATA, M. KOUCHI, and H. MIZOGUCHI, "Human Finding and Body Property Estimation by using Floor Segmentation and

3D Labelling," in *Proceedings of 2004 IEEE International Conference on Systems, Man & Cybernetics(SMC04)*, October 2004, pp. 2924–2929.

5. S. Kagami, Y. Takaoka, Y. Kida, K. Nishiwaki, and T. Kanade, "Online dense local 3d world reconstruction from stereo image sequences," in *Proceedings of 2005 IEEE/RSJ International Conference on Intelligent Robots and Systems(IROS2005)*, August 2005, pp. 2999–3004.

6. S. Thompson and S. Kagami, "Humanoid robot localisation using stereo vision," in *Proceedings of 2005 5th IEEE-RAS International Conference on Humanoid Robots(Humanoids2005)*, December 2005, pp. 19–25.

7. Y.Takahashi, K.Nishiwaki, S.Kagami, H.Mizoguchi, and H.Inoue, "High-speed pressure sensor grid for humanoid robot foot," in *Proceedings of 2005 IEEE/RSJ International Conference on Intelligent Robots and Systems(IROS2005)*, August 2005, pp. 1097–1102.

8. J. Chestnut, J. J. Kuffner, K. Nishiwaki, and S. Kagami, "Planning biped navigation strategies in complex environments," in *IEEE International Conference on Humanoid Robots (Humanoids2003)*, 10 2003.

9. S.Kagami, J.J.Kuffner, K.Nishiwaki, K.Okada, M.Inaba, and H.Inoue, "Humanoid arm motion planning using stereo vision and rrt search," *Journal of Robotics and Mechatronics*, vol. 15, no. 2, pp. 200–207, 2003.

10. M. Stilman and J. Kuffner, "Navigation among movable obstacles: Real-time reasoning in complex environments," *International Journal of Humanoid Robotics*, vol. 2, no. 4, pp. 479–504, December 2005.

11. L. Guilamo, J. Kuffner, K. Nishiwaki, and S. Kagami, "Manipulability optimization for trajectory generation," in *Proceedings of 2006 IEEE International Conference on Robotics and Automation(ICRA2006)*, May 2006, pp. 2017–2022.

12. K. Nishiwaki, M. Kuga, S. Kagami, M. Inaba, and H. Inoue, "Whole-body cooperative balanced motion generation for reaching," pp. 437–457, 2005.

13. K. Nishiwaki, Y. Fukumoto, S. Kagami, M. Inaba, and H. Inoue, "Object manipulation by hand using whole-body motion coordination," in *Proceedings of the IEEE International Conference on Mechatronics & Automation(ICMA2005)*, August 2005, pp. 1778–1783.